Supporting Information

Primary Tumor and Pre-metastatic Niches Co-targeting "Peptides-Lego" Hybrid Hydroxyapatite Nanoparticles for Metastatic Breast Cancer Treatment

*Hui Xiong[a], Shi Du[a], Ping Zhang[a], Zhijie Jiang[a], Jianping Zhou[a], Jing Yao[a]**

[a]State Key Laboratory of Natural Medicines and Jiangsu Key Laboratory of Druggability of Biopharmaceuticals, Department of Pharmaceutics, China Pharmaceutical University, 24 Tongjiaxiang, Nanjing 210009, China

* Correspondence to: Jing Yao, E-mail: yaojing@cpu.edu.cn (J. Yao).

As depicted in **Figure S1**, compared to the spectrum of PMC, the peaks of PH at 2.7ppm(q,1H,CH_2) and 8.15ppm(s,1H,NH) were assigned to -CH_2 linked to new formed amide bond and -NH of generated amide bond, respectively [1]，indicating the successful connection of PMC and HP by amide bond. Besides, in the FI-IR analysis, compared to the PMC, the characteristic peaks of carboxyl in PMC observed at 1782.3cm^{-1}(m, ν(C=O)) and 2564.6 cm^{-1} (w, ν（OH）) vanished in the spectrum of PH. In addition, peak at 1689.6 cm^{-1}(s, ν(C=O)) of PH was assigned to the newly formed amide bond (**Figure S2**). Besides, the peak at 601.5 cm^{-1}(m,β(P-O)) and 576.5cm^{-1}(m, β(P-O)) were the characteristic peaks of

$PO_4^{3-}$of HP, further confirming that PMC had coated on the surface of HP successfully.

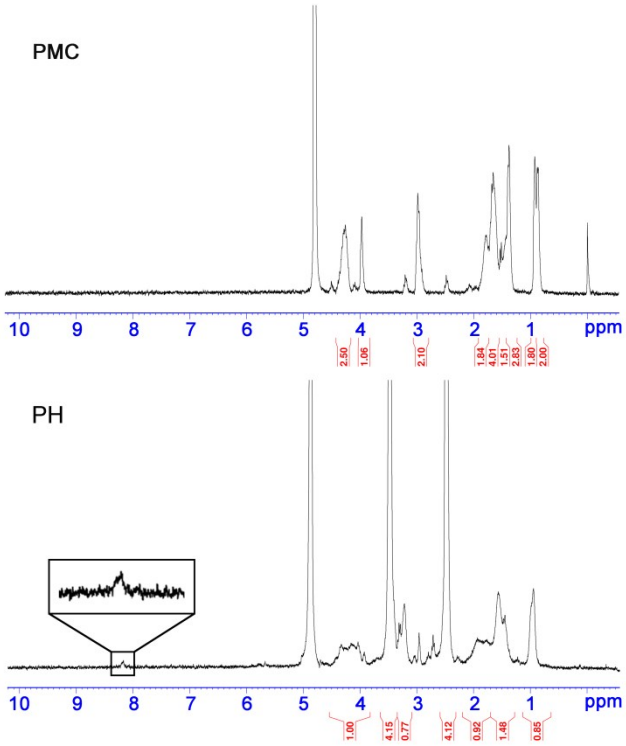

Figure S1. The ^1H NMR(300MHz, D_2O) spectrums of PMC and PH.

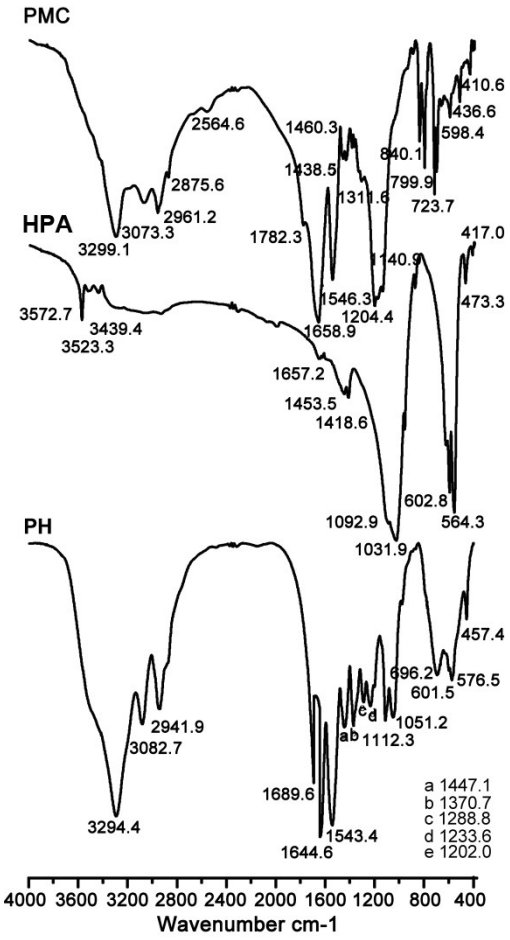

Figure S2. The FT-IR(KBr) spectrums of PMC,HPA and PH.

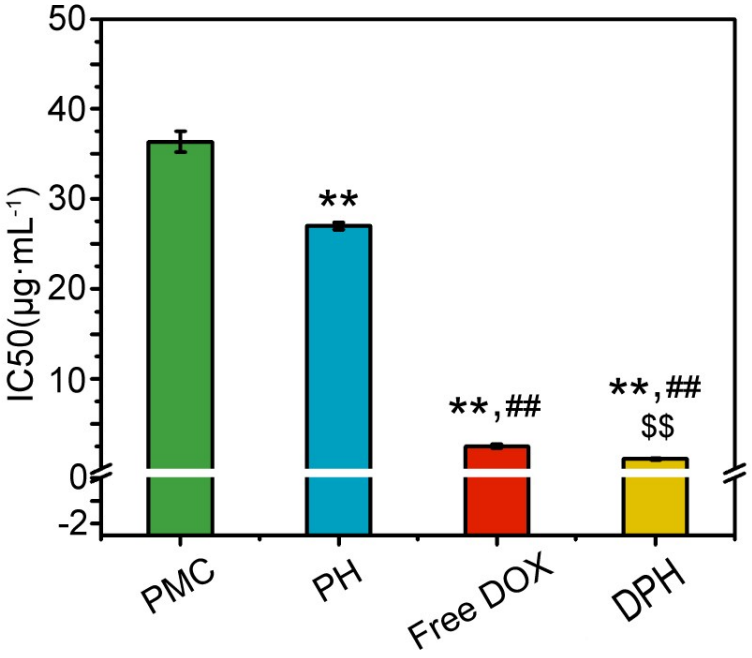

Figure S3. The IC50 of PMC, PH, Free DOX and DPH. Error bars indicated s.d. (n= 6). P value: **P <

0.01 *vs.* the control group; $^{\#\#}$P<0.01 *vs.* PH and $^{\$\$}$P<0.01 *vs.* Free DOX.

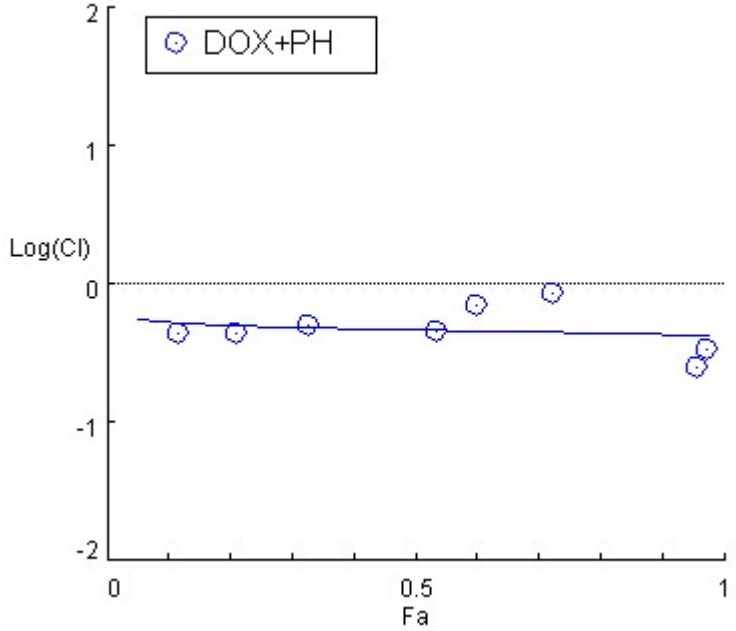

Figure S4. Logarithmic combination index plot for combination use DOX and PH.

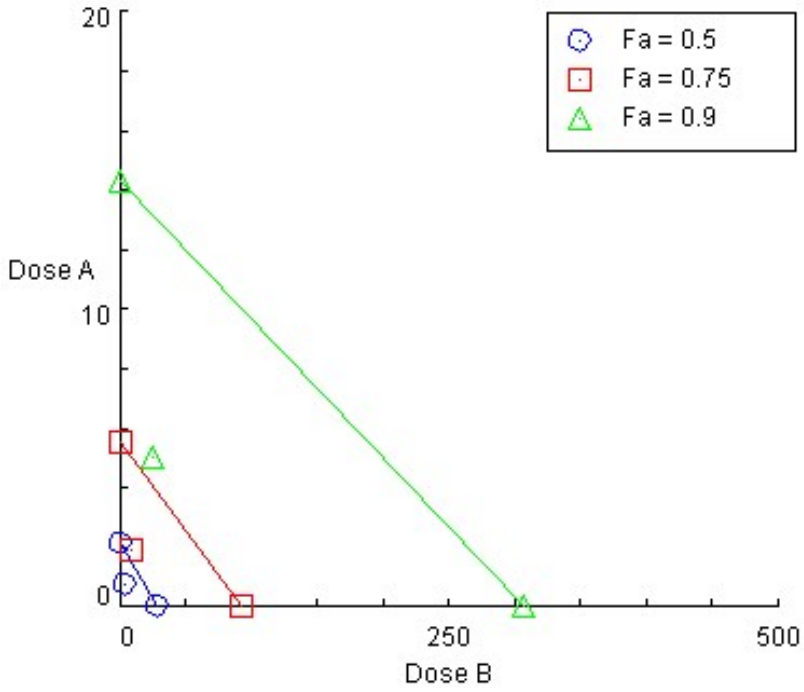

Figure S5. Isobologram for Combo: DOX(Dose A) and PH(Dose B) (DOX+PH [1:5]).

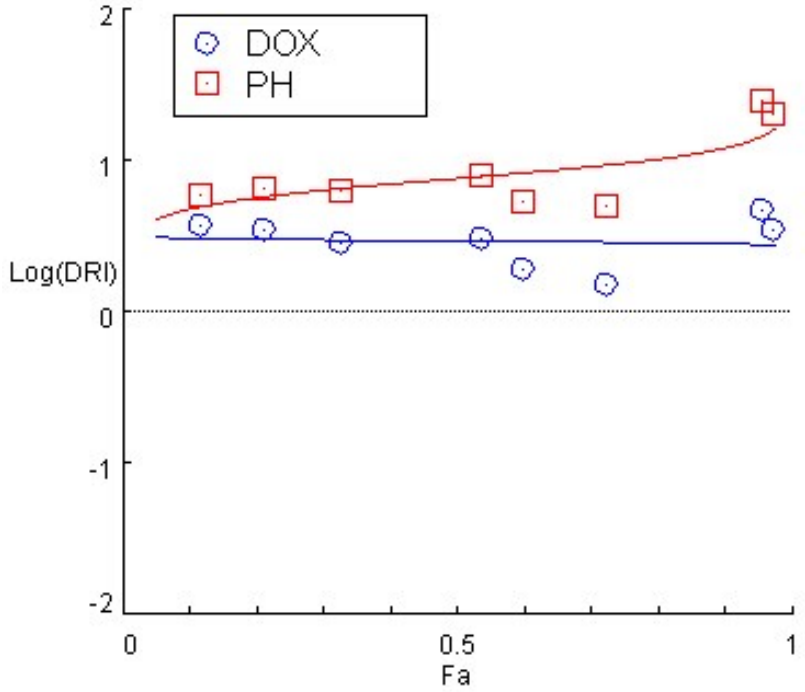

Figure S6. Log(DRI) Plot for Combo: DOX and PH (DOX+PH [1:5]).

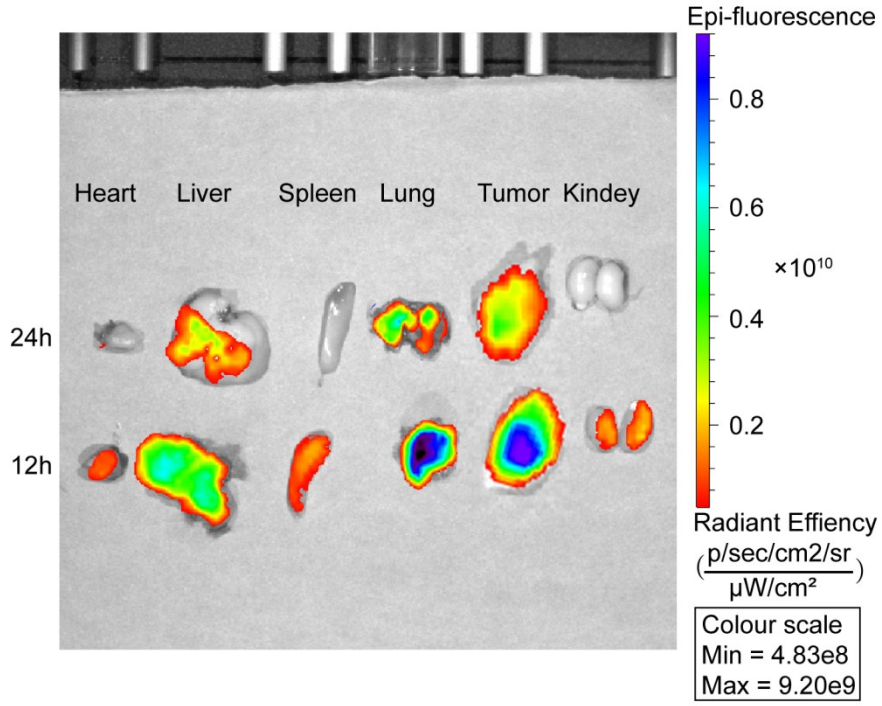

Figure S7. *Ex vivo* fluorescence imaging of the tumor and tissues harvested from the euthanized 4T1 aggressive lung metastasis mice at 12 h and 24 h post injection.

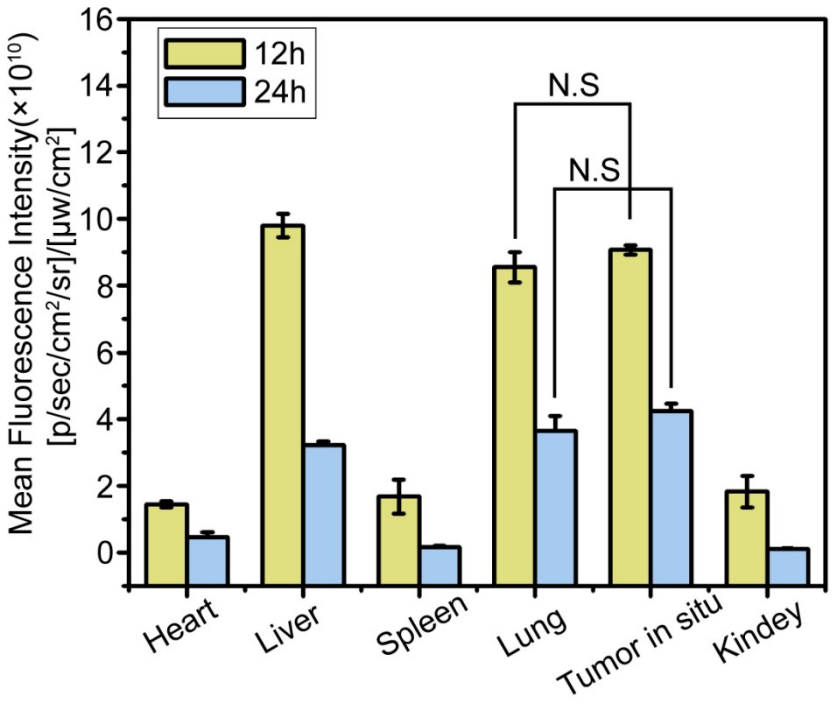

Figure S8. Region-of-interest analysis of fluorescent signals from the tumors and normal tissues. Error bars indicated s.d. (n= 3).

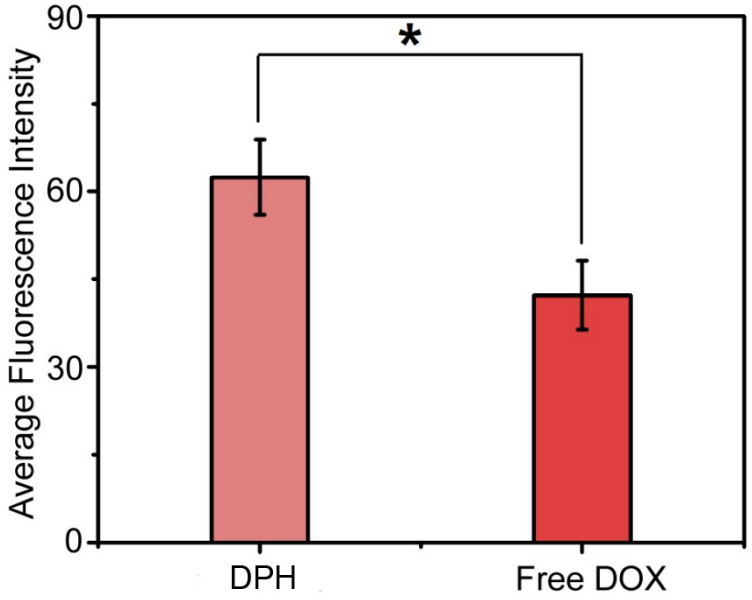

Figure S9. Average fluorescence intensity of lung micrometastasis after injection of DPH and Free DOX. Error bars indicated s.d. (n= 3).

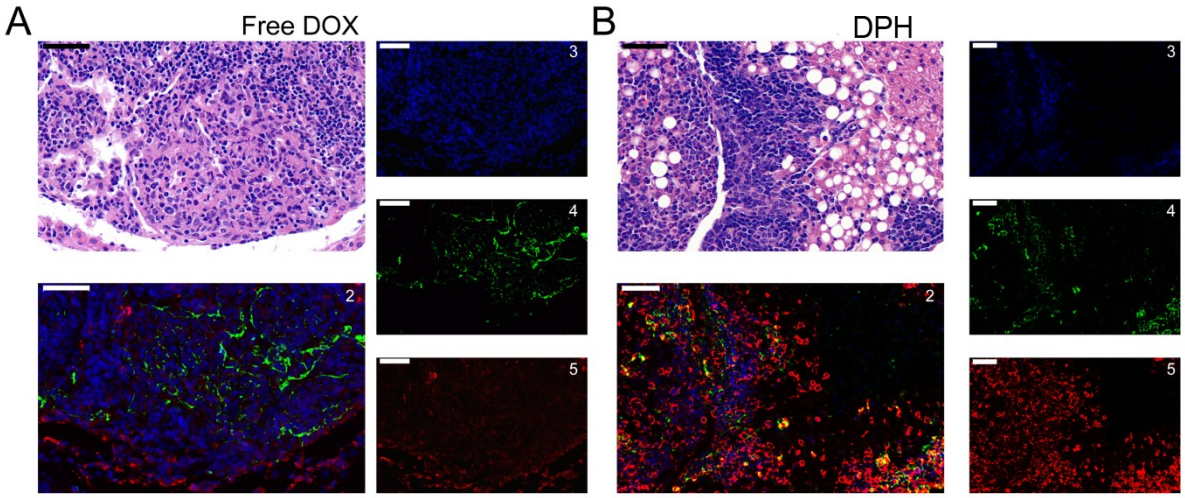

Figure S10. (A) Frozen sections of lung micrometastasis after injection of free DOX. (B) Frozen sections of lung micrometastasis after injection of DPH. 1: The HE images for indicating the micrometastasis location; 2:Merged images of different Fluorescent channels; 3: DAPI(Blue); 4:FN(Green); 5: Free DOX or DOX-PH(Red).Scale bars are 50 μm.

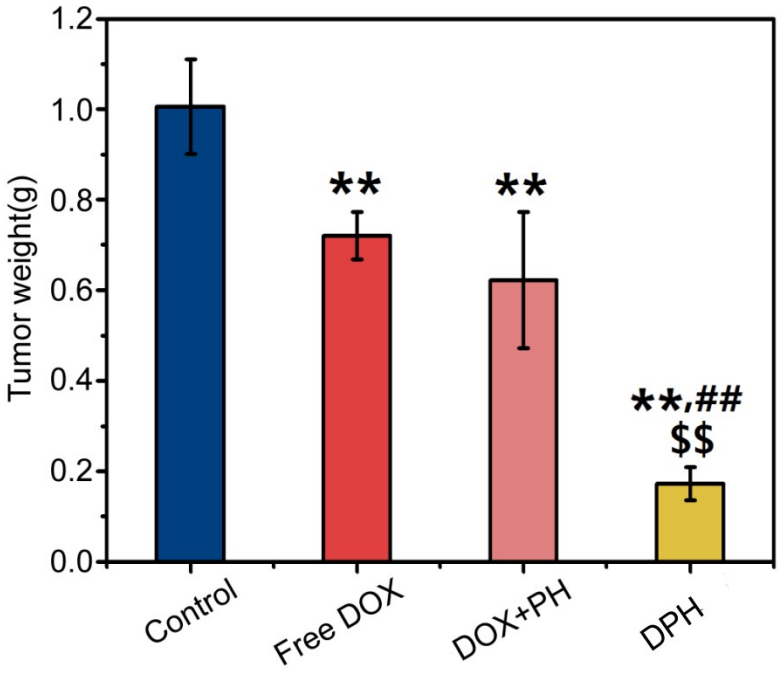

Figure S11. The primary tumor weight of 4T1 aggressive lung metastasis mice after treatment of 5% glucose, Free DOX , DOX+PH and DPH group. Error bars indicate s.d. (n = 5). P value: $^{**}P < 0.01$ *vs.* the control group; $^{\#\#}P<0.01$ *vs.* Free DOX and $^{\$\$}P<0.01$ *vs.* DOX +PH.

Table S1. Tumor inhibition ratio observed in 4T1 orthotopic implantation tumor-bearing mice treated with Free DOX, DOX+PH, DPH and 5% Glucose . Error bars indicated s.d. (n= 5). $^{\#\#}$P<0.01 *vs.* Free DOX and $^{\$}$P<0.05 *vs.* DOX + PH.

Groups	Inhibition ratio (%)
Control	-
Free DOX	28.41±6.11
DOX+PH	38.09±4.98
DPH	82.82±7.02$^{\#\#,\$}$

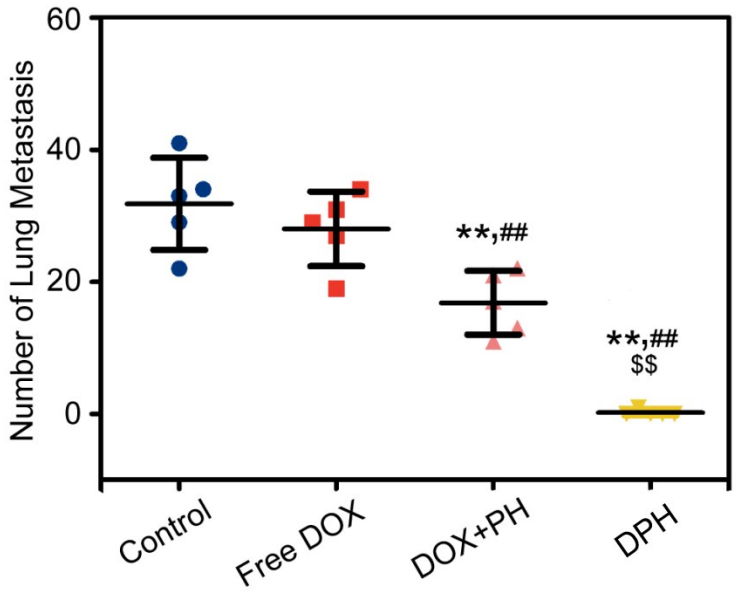

Figure S12. The number of visually detected metastatic nodules in lungs from different groups. Error bars indicate s.d. (n = 5). P value: **P < 0.01 *vs.* the control group; $^{\#\#}$P<0.01 *vs.* Free DOX and $^{\$\$}$P<0.01 *vs.* DOX +PH.

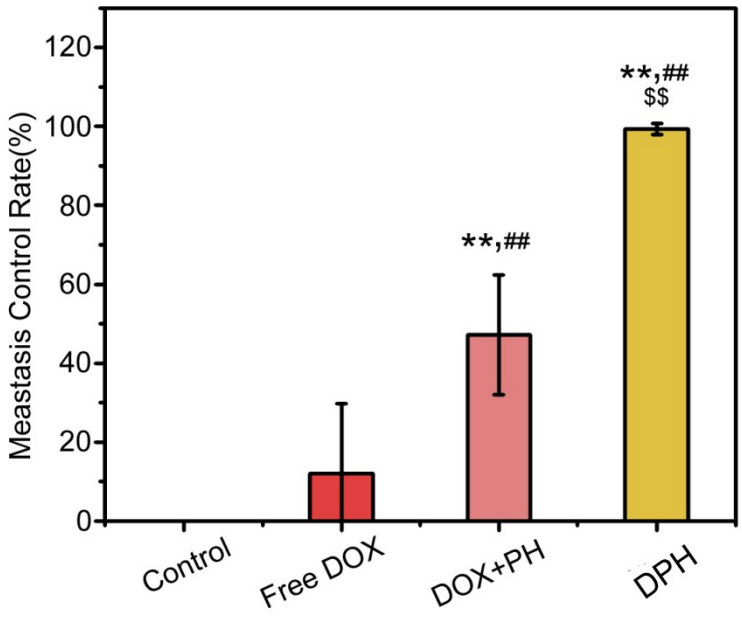

Figure S13. The metastasis control rate of different groups. Error bars indicate s.d. (n = 5). P value: $^{**}P < 0.01$ *vs.* the control group; $^{\#\#}P<0.01$ *vs.* Free DOX and $^{\$\$}P<0.01$ *vs.* DOX + PH.

It is worth noting that the side effects of DOX, such as cardiotoxicity and chemotherapy-induced liver injury limited its clinical application and reduced the compliance of patient severely [2-4]. Therefore, we investigated the potential toxicity of this system. The well maintained mouse weight throughout the treatment indicated that DPH held alleviated toxicity compared to the free DOX (**Figure S14A**). Besides, the decreased serum creatine kinase (CK) level (**Figure S14B**) and effective ameliorated heart tissue injure (**Figure S14C**) demonstrated that DPH could nearly avoid the risk of cardiotoxicity caused by DOX. In the evaluation of liver toxicity, DPH also displayed striking catabatic hepatotoxicity, which was specifically manifested in remarkable reduced serum levels of aspartate transaminase (AST) and alanine aminotransferase (ALT) (**Figure S14D**) as well as mitigatory liver tissue injure(**Figure S14C**). These reduced hepatotoxicity might be closely related to HP which had the potential to selectively assault liver tumor cells without damaging normal liver cells [4].

All these results suggested that DPH possessed intensive primary tumor and micrometastasis inhibition efficacy with reduced side effects.

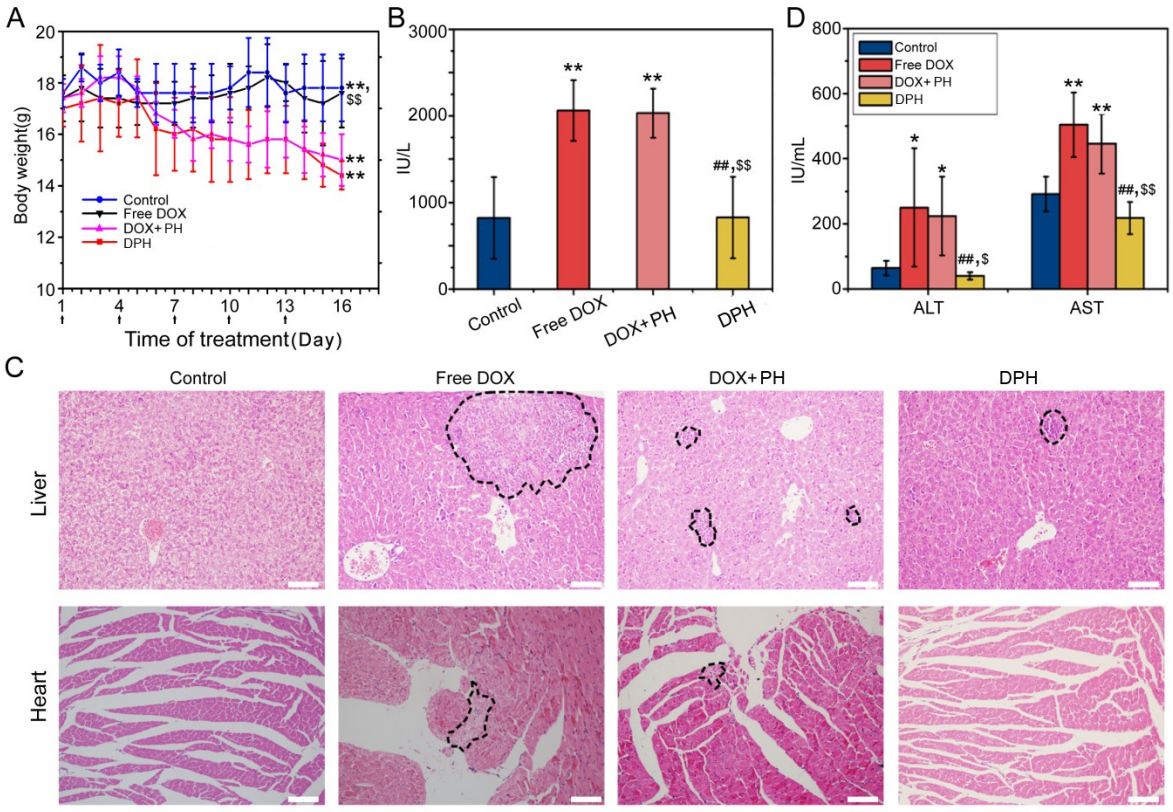

Figure S14. (A) The body weight variation of tumor-bearing mice during treatment. Error bars indicate s.d. (n = 5). (B) The changes of serum CK levels of 4T1 orthotopic implantation tumor-bearing mice. Error bars indicate s.d. (n = 5). (C) Representative images of paraffin-embedded liver and heart sections after HE staining. The black circles indicate the sites of injury. Scale bars are 50μm. (D)The changes of serum AST and ALT levels of 4T1 orthotopic implantation. Error bars indicate s.d. (n = 5). $^{\#\#}P<0.01$ *vs.* Free DOX and $^{\$}P<0.05$, $^{\$\$}P<0.01$ *vs.* DOX + PH. P value: $^{*}P < 0.05$, $^{**}P < 0.01$ *vs.* the control group; $^{\#\#}P<0.01$ *vs.* Free DOX and $^{\$}P<0.05$, $^{\$\$}P<0.01$ *vs.* DOX + PH.

References

1. J. Pieper, K. H. Ott and B. Meyer, *Nat. Struct. Biol*, 1996, 3, 228-232.
2. T. Tian, J. Li, M. Y. Wang, X. F. Xie and Q. X. Li, *Eur. J. Pharmacol*, 2012, 683, 246.

3. S. Yilmaz, A. Atessahin, E. Sahna, I. Karahan and S. Ozer, *Toxicology*, 2006, 218, 164-171.
4. Y. Yuan, C. Liu, J. Qian, J. Wang and Y. Zhang, *Biomaterials*, 2010, 31, 730-740.